



This is a repository copy of *Investigation of surface deposition in a simulated fuel injector feed arm with sudden expansion/contraction*.

White Rose Research Online URL for this paper:  
<http://eprints.whiterose.ac.uk/115339/>

Version: Accepted Version

---

**Article:**

Alborzi, E., Blakey, S., Ghadbeigi, H. [orcid.org/0000-0001-6507-2353](https://orcid.org/0000-0001-6507-2353) et al. (2 more authors) (2016) Investigation of surface deposition in a simulated fuel injector feed arm with sudden expansion/contraction. *Fuel*, 186. pp. 534-543. ISSN 0016-2361

<https://doi.org/10.1016/j.fuel.2016.08.080>

---

Article available under the terms of the CC-BY-NC-ND licence  
(<https://creativecommons.org/licenses/by-nc-nd/4.0/>)

**Reuse**

Unless indicated otherwise, fulltext items are protected by copyright with all rights reserved. The copyright exception in section 29 of the Copyright, Designs and Patents Act 1988 allows the making of a single copy solely for the purpose of non-commercial research or private study within the limits of fair dealing. The publisher or other rights-holder may allow further reproduction and re-use of this version - refer to the White Rose Research Online record for this item. Where records identify the publisher as the copyright holder, users can verify any specific terms of use on the publisher's website.

**Takedown**

If you consider content in White Rose Research Online to be in breach of UK law, please notify us by emailing [eprints@whiterose.ac.uk](mailto:eprints@whiterose.ac.uk) including the URL of the record and the reason for the withdrawal request.



[eprints@whiterose.ac.uk](mailto:eprints@whiterose.ac.uk)  
<https://eprints.whiterose.ac.uk/>

# Investigation of Surface Deposition in a Simulated Fuel Injector Feed Arm with Sudden Expansion/Contraction

Ehsan. Alborzi<sup>1</sup>, Simon. Blakey, Hassan. Ghadbeigi, Christophe. Pinna,  
Christopher. Lewis

*Department of Mechanical Engineering, The University of Sheffield, Sheffield, England*

---

## Abstract

Formation of surface carbonaceous deposits at inner surface of two classes of simulated jet engine burner feed arm including a straight tube as well as two tubes with sudden expansion/contraction was studied using “Aviation Fuel Thermal Stability Test Unit(AFTSTU)”. The generated results indicate that phenomena such as stagnant flow formation, flow separation and vena contracta have a substantial impact on surface deposition. Commercial “Computational Fluid Dynamics(CFD)” package, ANSYS Fluent was used to interpret the impact of flow features and heat transfer characteristics on surface deposition. The experimental data obtained in this work were used in a one dimensional heat transfer model for prediction of deposit thickness in simulated burner feed arms. Subsequently, the simulated burner feed arm with contraction/expansion structure were sectioned and prepared for deposit visualisation with “Scanning Electron Microscopy(SEM)”. The results of visualised deposits are consistent with one dimensional heat transfer calculation.

The novel set of experimental data presented in this work provides a basis for the construction of predictive models for calculation of deposit growth and total deposit mass in fuel injection system. A description of the model will be addressed in the second paper of this work which is currently under preparation.

*Keywords:* Aviation fuel, Burner feed arm, Fuel Injection System, Thermal oxidative stability, Surface deposition

---

\*Corresponding author

*Email address:* e.alborzi@sheffield.ac.uk (Ehsan. Alborzi)

## Nomenclature

$\delta_t$  wall temperature at time t( $\mu\text{m}$ )

$a$  an empirical correction factor based on previous experimental data

$h_{fuel}$  convective heat transfer coefficient of jet fuel( $\text{W}/\text{m}^2\text{K}$ )

$T_0$  wall temperature at time zero(k)

$T_t$  wall temperature at time t(K)

$T_{bulk}$  bulk fuel temperature(k)

## 1. Introduction

Aviation gas turbine fuel is exposed to thermal stresses as it is used as a heat sink for the engine lubricating system on route from the fuel tank, through the engine, to the combustion chamber. The temperature rise as the fuel passes through the engine causes a range of reactions in the fuel which results in the formation of soluble and insoluble particulates [1, 2]. These changes in chemical structure can limit the performance of filters and burner feed arms, cause disruption to the flow of fuel, and result in a reduction in the performance of specific engine components [3, 4]. Advanced aviation engine technologies place an increasing requirement on the fuel to act as a heat sink. The trend to higher pressure ratio engines presents a twofold challenge to the use of the fuel as a heat sink: Firstly, higher pressure ratios result in an increased thermal load on the engine lubrication system, which in turn increases the heat sink requirements. Secondly, the higher pressure ratios increase the thermal efficiency of the cycle, which results in a lower fuel flow rate. In addition, hot air discharges from the compressor at a high velocity and flows around the burner feed arm, through which fuel passes on its path to the atomizer. This results in a high rate of convective heat transfer into the burner feed arm and flow passages around the swirlers and flow features in next generation, lean burn and staged combustion injectors. These more severe conditions have the potential to result in an increased level of thermal degradation reactions which ultimately lead to the formation of carbonaceous deposits on the fuel wetted surfaces.

The formation of surface carbonaceous deposits is a result of the simultaneous physico-chemical interactions governed by multitude of variables including chemical composition of jet fuel, bulk fuel temperature, wall temperature, duration of thermal exposure, flow regime, physico chemical characteristics of the fuel wetted surfaces and surface roughness amongst others [1]. A representative test for the studying of surface deposition at full scale (equivalent to say 10,000 hours of flight, in which time deposit may have started to effect engine performance) which matches these variables is remarkably costly due to the fuel volumes and test time required therefore compromises in the scaling of the investigation are required [4]. As a consequence, any conclusions or design rules developed from the results in a simplified experiment and extrapolated to in service conditions needs to be rigorously evaluated for their validity.

Previous works on the impact of both laminar [5, 6] [7, 8] and turbulent fluid flow [4, 9, 10] on jet fuel autoxidative deposition have been published using a simple straight cylindrical tubing of a constant diameter. However, in many current and future fuel injector designs, the fuel passageways of the burner feed arm and the injector are far from this simple case and include geometric features such as: bends, annular regions, multiple parallel paths, features to introduce swirlers and large expansions and contractions in the flow. Jiang et.al. [11] used a geometry composed of a sudden expansion or contraction to investigate the effect of flow path changes on fuel autoxidation and deposition under laminar flow regime in a near isothermal tube reactor. The complex geometrical features create complex flow regimes, potentially including eddies, secondary flows and vena contracta which substantially affect the heat transfer rate at fuel wetted surfaces where deposits may form.

The optimal design and planned maintenance of the new injectors requires a theoretical framework for the robust estimation of surface deposition with respect to the complexities caused by the geometrical features in jet engine representative condition. The work presented here provides a novel set of experimental data corresponding to the surface deposit formation in two different designs of jet engine burner feed arms; a pipe with a sudden expansion/contraction and for comparison, a straight tube, under engine representative conditions, simulated by AFTSTU. The rig is a pilot scale experimental unit [9] capable of assessing the interaction of a simulated engine fuel system and a representative fuel. The AFTSTU simulates conditions in a range of current and future aero engines ensuring that the fuel arrives at a simplified burner feed arm in a representative condition to that in service, which is critical in assessing the likely interaction with hot surfaces and flowing fuel.

The experimental data provides a basis for the validation of a mathematical model for prediction of deposit growth and total deposit mass in a modelled fuel injection system. A description of the model and implementation in a transient CFD simulation is addressed in the second paper of this work which is currently under preparation.

## 2. Experimental Work

### 2.1. Fuel and fuel thermal history

Inside the rig, the thermal regimes from the fuel tank to the burner feed arm are replicated in a modular fashion, allowing for independent control of the heat loading within the various sections of the rig as shown in figure 1. A representative Jet A-1 fuel was tested in three experiments with AFTSTU. The composition of major hydrocarbon constituents and some of the heteroatomic species along with the corresponding quantification methods are presented in table 1.

The fuel sample was analysis externally using an in house method as developed by Intertek. This method determines sulfur containing compounds and group types in middle distillates using an Agilent 7890 N “Gas Chromatograph(GC)” equipped with a Zoex thermal modulation and an Agilent 355 sulfur chemiluminescence detector. Quantification of sulfur classes was carried out by the normalization to the total sulfur content as determined by combustion followed by UV-Fluorescence. The  $GC \times GC$  analysis separates sulfur-containing compounds according to their boiling point and upon their polarity. Thus it was possible to elute the benzothiophenes and dibenzothiophenes in two well-defined bands clearly separated from the band of thiophenes, sulfides and mercaptans. Hydrocarbon speciation was carried out using “UOP Method 990-11”. This method determines molecular type homologous series by carbon number.

It was assumed that the concentration of dissolved oxygen in the jet fuel to be around 70 ppm, in line with [12, 5, 6, 7, 8].

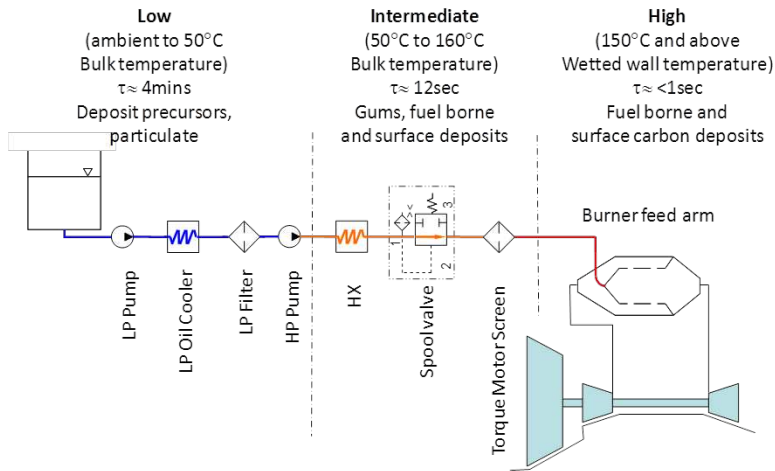


Figure 1: Simplified schematic of the AFTSTU rig modules

Chemical species	Concentration	Units	Methods
n-Praffins	20.67	% m/m	$GC \times GC - FID(UOP990)$
iso-Praffins	24.77	% m/m	$GC \times GC - FID(UOP990)$
Cyclics	30.84	% m/m	$GC \times GC - FID(UOP990)$
Alkylbenzenes	16.18	% m/m	$GC \times GC - FID(UOP990)$
Benzene	0.01	% m/m	$GC \times GC - FID(UOP990)$
Toluene	0.21	% m/m	$GC \times GC - FID(UOP990)$
Indans and tetralins	5.15	% m/m	$GC \times GC - FID(UOP990)$
Naphtalenes	1.33	% m/m	$GC \times GC - FID(UOP990)$
Antioxidant	25	mg/l	$GC \times GC - FID(UOP990)$
Total Sulfur	1400	mg/Kg	$GC \times GC - SCD$
Thiols, Sulfides and Disulfides	210	mg/Kg	$GC \times GC - SCD$
Total Hydroperoxides	4.7	$\mu M$	West et.al [13]
Dissolved metals	52	mg/kg	MT/ELE/15

Table 1: Composition of major hydrocarbon and some of the heteroatomic species quantified in tested fuel

## 2.2. Burner feed arm design and Test conditions

A series of three burner feed arm tests were carried out, the first(test1) ran a straight pipe simulated burner feed arm, the second test(test2) carried out with the replicated feed arm with sudden expansion/contraction structure. The total deposited carbon in test1 and test2 was quantified by carbon burn off analysis. As carbon burn off is a destructive method, test2 was repeated, and alternatively, the tube was sectioned for the purpose of deposit visualisation with optical microscope(test3).

All burner feed arms were manufactured from cold drawn 316 stainless steel tube. The simple straight tube (test1) was made from a single tube, 6 mm

od, 2 mm id. Three pairs of K-type sheathed thermocouples were silver brazed into the wall of the tube. The three outer thermocouples were 0.2 mm from the outer tube surface while the three inner thermocouples were 0.4 mm distant from the inner tube surface. This standard design was adapted to accommodate a pipe with expansion/contraction features by fitting tubes of different diameters together concentrically. As the fuel pressure in the “High Pressure (HP)” system of the rig was of the order of 500 psi, it was seen to be preferable to contain any internal changes inside a continuous tube shell rather than cut and weld sections of pipework together.

In order to fit within the existing heater coil, the external diameter of any burner feed arm unit was limited to 8 mm od. Due to the range of cold drawn tubing available, an 8.1 expansion ratio and a 0.742 contraction ratio within an 8 mm external diameter were chosen. In a region of 15 mm either side of the pipe, the tubes were prepared to an interference fit when pressed together. This was to ensure good thermal contact between the layers. The interference fit deformed the outer diameter of the 8 mm tube in the interference region and required post assembly machining of the outer tube to bring the external diameter of the nozzle back to within 8 mm. In order to ensure a sharp edge to the step change in diameter in the composite tubes, the inner tubes of identical length were assembled first and then machined to produce a surface normal to the tube center line at the step edge, before being cooled and assembled into the larger diameter tube. As the inner tubes are visible at the inlet and outlet of the nozzle tube, it was possible to confirm good alignment of the edge in the test section.

The detailed design of both burners feed arm geometries are presented in figure 2. A “Radio Frequency(RF)” induction heating coil with a total length of 120 mm was centred on the central pair of thermocouples. Induction heating is mostly a skin effect where electromagnetic field is only present in the first millimetres of the heated specimen. Therefore, at the operating frequency of the heater around 280 kHz, 87% of the power was dissipated in less than the first 0.6 mm of the outer surface. [14]

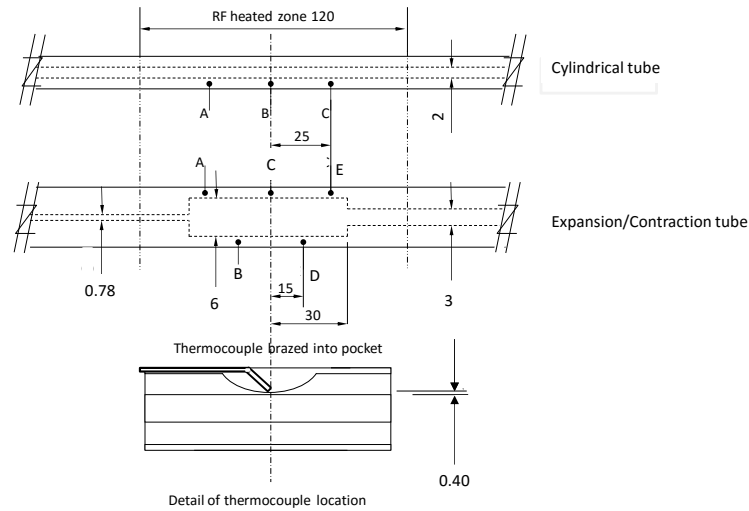


Figure 2: Comparison between standard and contraction/expansion nozzle and thermocouple positioning (not to scale, dimensions in mm)

Prior to each test, the replicated feed arms were treated with a mixture of weak hydrofluoric and nitric acids solution to clean the internal surface of the tubes to achieve a repeatable surface finish. The tubes were initially heated to a predetermined temperature. During this phase the temperature was controlled at the inner wall by the thermocouple B (in cylindrical tube) and thermocouple C (in expansion/contraction tube). This allowed to check the performance of the nozzle during the warm up period. It was observed that for a given inductive power, the temperature at the thermocouple B (in test 1) and thermocouple C (in test 2 and 3) was 250 °C. At this temperature, the temperature difference between the inlet and outlet increased by approximately 10 °C. Therefore, once steady state heat transfer was achieved the heating power was fixed for the corresponding temperature. A summary of the test conditions is presented in table 2.

Test initial conditions	Test1	Test2	Test3
Flow Rate(l/h)	23	23	23
Pressure in low pressure(LP) system(psi)	50	50	50
Temperature in low pressure(LP) system( $^{\circ}$ C)	50	50	50
Pressure in high pressure(HP) system(psi)	500	500	500
Temperature in High(HP) system( $^{\circ}$ C)	180	180	180
Test Duration(h)	25	25	25
Initial Wall temperature( $^{\circ}$ C)	25	25	25

Table 2: Test conditions in AFTSTU

### 2.3. Post test analysis methods

- **Carbon burn off**

The replicated burner feed arms in test1 and test2 were placed in a 50 mm long tube furnace at  $650^{\circ}$ C with a constant flow of hydrocarbon free air passing through them. In this condition, the reaction of carbon and oxygen was initiated in the air, yielding carbon dioxide and carbon monoxide which then passed through a catalytic furnace to complete its oxidation. The concentration of carbon dioxide and carbon monoxide produced in each tube was then quantified using a non-dispersive infra-red gas analyser. The amount of carbon was then calculated from the measured concentrations and the air flow rate. The repeatability of this technique is  $\pm 5\%$  or 0.1 mg whichever is greatest. The Carbon Burn off method is based on the assumption that the major constituents of surface deposits are carbonaceous materials, which is largely valid [1]. In order to gain some spatial resolution along the axis of the tubes, zonal carbon burn off analysis was carried out using four segments of the tubes. The position of these segments are shown in figures 11a and 11b in results and discussion section.

- **Deposit thickness direct measurement**

As an alternative to the carbon burn off method, it is possible to section the tubes and inspect the deposit thickness at certain sections using optical microscope techniques. In order to preserve the initial structure of the deposited layer, care needs to be taken in the preparation stages. For this reason, a precision cutting machine (Buehler Isomet) was used to cut the specimen with a speed of 2 mm/min using diamond wafering blades. In order to minimise the risk of deposit structural change due to heating in the course of cutting, a water based cutting fluid (Iso-cut Plus) was used. The tube sections were then cold mounted in a standard cylindrical mould using epoxy resin followed by the vacuum impregnation. The resin was left to cure for about 10 h to obtain a solid

resin mould. The vacuum impregnation process was to ensure that no air is left in the mounted specimen and the resin completely filled up the porous structure of the deposit. The mounted specimens were then mechanically polished to obtain a flat scratch free surface that enables cross sectional analysis of the deposited tube. The mechanical polishing started using rough abrasive papers to very fine polishing with 1  $\mu\text{m}$  diamond paste for the final polishing step to create a mirror polished surface. The specimens were washed thoroughly with water and dried with a hot air blower after each polishing step to avoid contamination of the surface.

- **Analytical method- 1D heat transfer analysis**

As shown in equations 1 and 2, a simplistic one dimensional heat transfer analysis was used to calculate the deposit thickness at certain locations along the heated tube corresponding to the thermocouple tips where the temperature rise data were logged. Assuming no axial effects, if the bulk fuel temperature rise throughout the testing can be shown to be constant, then the heat flux through the wall of the tube will also be constant.

$$\frac{T_0 - T_{bulk}}{\frac{1}{h_{fuel}}} = \frac{T_t - T_{bulk}}{\frac{1}{h_{fuel}} + \frac{\delta_t}{k}} \quad (1)$$

Where  $T_0$  is the wall temperature at time zero and  $T_t$  represents the wall temperature at time t.  $\delta_t$  is the deposit thickness at time t,  $h$  denotes the convective heat transfer coefficient and k represents thermal conductivity of deposited materials. Therefore the calculation of deposit thickness can be reduced to a function of the change in wall temperature,  $T_t - T_0$ :

$$\delta_t = a \frac{k(T_t - T_0)}{h(T_0 - T_{bulk})} \quad (2)$$

Where  $a$  is an empirical correction factor based on previous experimental data to account for the morphology of the deposit layer.

Several studies have investigated the conductivity of typical deposits found in aviation fuel autoxidation test rigs of a range of scales. TeVelde and Glickstien [15] measured a strong variation in deposit conductivity with deposit thickness, varying by an order of magnitude between 0.017W/m<sup>2</sup>K to 0.17W/m<sup>2</sup>K between 20  $\mu\text{m}$  and 25  $\mu\text{m}$ . Earlier experimental work [16] on sectioned tubes from the AFTSTU using different

jet fuel type has suggested an estimated thermal conductivity of to  $0.012W/m^2K$  would be appropriate and was validated against microscope assessment of sectioned tubes from the rig. This agrees well with the work of Tevelde and Glickstein as the deposit was below  $20\mu m$  for the majority of the testing work. If a bulk fuel temperature is estimated from the bulk fuel temperature data, and a local value of  $h$  can be obtained from the steady state CFD simulation, the deposit thickness can be estimated from the wall temperature data alone. This allowed experimentally derived data to be compared directly to optical microscope images of the real deposit thickness.

### 3. Numerical Work

In order to assess the deposit growth rates using a numerical model, it is essential to ensure that the heat transfer model is accurate before the complexity of a chemically reacting and depositing flow is considered. A two dimensional, axis symmetric, steady state CFD simulation was performed to describe the flow field and heat transfer characteristics of non-reactive jet fuel passing through the expansion/contraction tube at the initial conditions of the experiment. As schematically shown in figure 3, the computational domain is divided in three regions including tube body(dark grey), flow region(blue) and the skin effect region(light grey) created by the RF heater unit. The tube is surrounded by ambient air as per the experimental setup. The flow region is bounded by the inlet and outlet boundaries and flow enters at the left and exits at the right boundary. For a better computational grid quality, the flow domain was subdivided in several connected rectangular blocks and the structured grids were created for each block accordingly. For each rectangular block an orthogonal ( $90^\circ$ ) grid in a Cartesian Coordinate framework was used and the attachment of each face of adjacent block was regular.

The tube inlet boundary was located 100 mm upstream of the heated region in order to ensure that the fluid velocity and thermal profiles fully developed radially. The thermal and momentum boundary conditions at the inlet for both cylindrical and expansion/contraction tubes were set up to closely resemble the conditions presented in table 2. Accordingly, a mean inlet velocity equal to 1.57 m/s at a constant temperature of 453k was considered for the inlet of both tubes. At this condition, the Reynolds number is approximately equal to 10000 hence a turbulent intensity(10%) and hydraulic diameter was applied at inlet(both tubes). The outlet boundary condition for the cylindrical tube was located 250 mm downstream of the physical tube

inlet however as the step change in contraction section causes flow recirculation and vena contracta, the outlet boundary for the expansion/contraction tube was placed more than 10 times of the step height to ensure that interior solution was not affected by the location of the outlet boundary. The thermal properties of jet fuel as function of temperature including density, heat capacity, thermal conductivity and viscosity were taken from work published by Katta and Roquemore [17] for the range of 130–240°C. Thermal properties of the stainless steel were assumed constant and taken from Fluent property data base while the properties of the air surrounding the outer tube wall surface were based on the data from literature [18].

No slip condition was assumed for the wall boundaries corresponding to the fuel wetted surfaces. The thermal boundary condition at the inner walls was considered as coupled. The boundaries of the computational domain which correspond to the outer wall surfaces were considered as a heat flux generated by the convective and radiative heat transfer terms as presented in equation 3. [18]

$$Q = h(T_a - T_w) + \epsilon\sigma(T_a^4 - T_w^4) \quad (3)$$

Where  $\epsilon$  denotes the external emissivity which is 0.4 for most types of stainless steel,  $\sigma$  represents Stefan-Boltzmann constant equal to  $5.6703 \times 10^{-8} \text{ W/m}^2\text{K}^4$ ,  $T_a$  is ambient temperature equal to 298 k.  $T_w$ , the outer wall temperature alongside the tube was unknown, therefore a user defined function was created to extract the temperatures from each computational cell at the outer wall of the tube. The external natural convection heat transfer was calculated to be  $13.94 \text{ W/m}^2\text{K}$ .

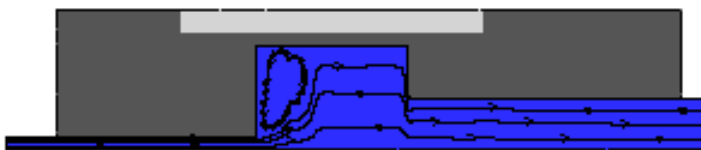


Figure 3: The computational domain of replicated feed arm with contraction/expansion structure

Two turbulence models, standard  $k - \epsilon$  and  $k - \omega$  were used for the CFD simulation in this work. The  $k - \epsilon$  offers the simplest level of closure since it has no dependence on the geometry or flow regime input. Nonetheless, numerical constraints are identified especially for flows with large, rapid and extra

strains since the model generally fails to fully describe the subtle impacts of the streamline curvature on the turbulence. In the  $k - \omega$  like the standard  $k - \epsilon$ , a modelled transport equation is solved for  $\omega$  to determine its local distribution within the fluid flow. However, the model is highly sensitive to the free stream value of  $\omega$  and requires great care taken in setting this value to prevent spurious results for the boundary layer flow calculation. This is of great concern as physico-chemical interactions leading to the formation of surface carbonaceous deposits are much more pronounced in boundary layer region in comparison to the bulk fuel. In order to overcome such problems, Menters model with the shear stress transport (SST) was used in this work. This model combines both standard  $k - \epsilon$  and  $k - \omega$  models retaining the properties of  $k - \omega$  close to the wall and gradually blends into the standard  $k - \epsilon$  model away from the wall.

Since the application of wall functions is to relate the flow variables to the first computational grid point thus removing the requirement to resolve the structure in between, the first grid row needs to be carefully placed so that it does not fall into the viscous sub layer. Therefore, the aspect ratio for regions far from the fuel wetted surfaces was maintained within the range of  $2 < AR < 5$ . For near wall boundaries the values of AR were slightly greater than 5 due to the need for appropriate small  $\Delta x$  mesh spacing in the flow direction.

#### 4. Results and Discussion

During test1, the wall temperature increased over the thermal exposure time as shown in figure 4a. The results indicate that the highest temperature rise occurred at thermocouple C which was axially furthest along the heated section of the tube and the lowest temperature rise was recorded at thermocouple A, the closest to the beginning of the heated region. The temperature rise is attributed to the lower thermal conductivity of insulative layer of carbonaceous materials in comparison to the stainless steel. It is important to note that the multi-dimensional analysis of transient heat transfer in such a system including surrounding air, stainless steel, carbonaceous deposits and flowing bulk fuel is a complicated task. The precision of such analysis is limited to the accuracy with which the thermo physical properties of deposits are known.

The results of calculated deposit thickness using simplistic one dimensional heat transfuse analysis are shown in figure 4b. It can be seen that the formation of deposit over time follows the same trend as temperature rise

data. The results of temperature rise for the simulated feed arm with expansion/contraction corresponding to test2 are shown in figure 4c. It is observed that more pronounced temperature rise occurred at thermocouples E and C while thermocouples A, B and D did not record remarkable changes over the course of thermal exposure. The local deposit thickness for this tube was calculated using one dimensional heat transfer analysis and presented in figure 4d.

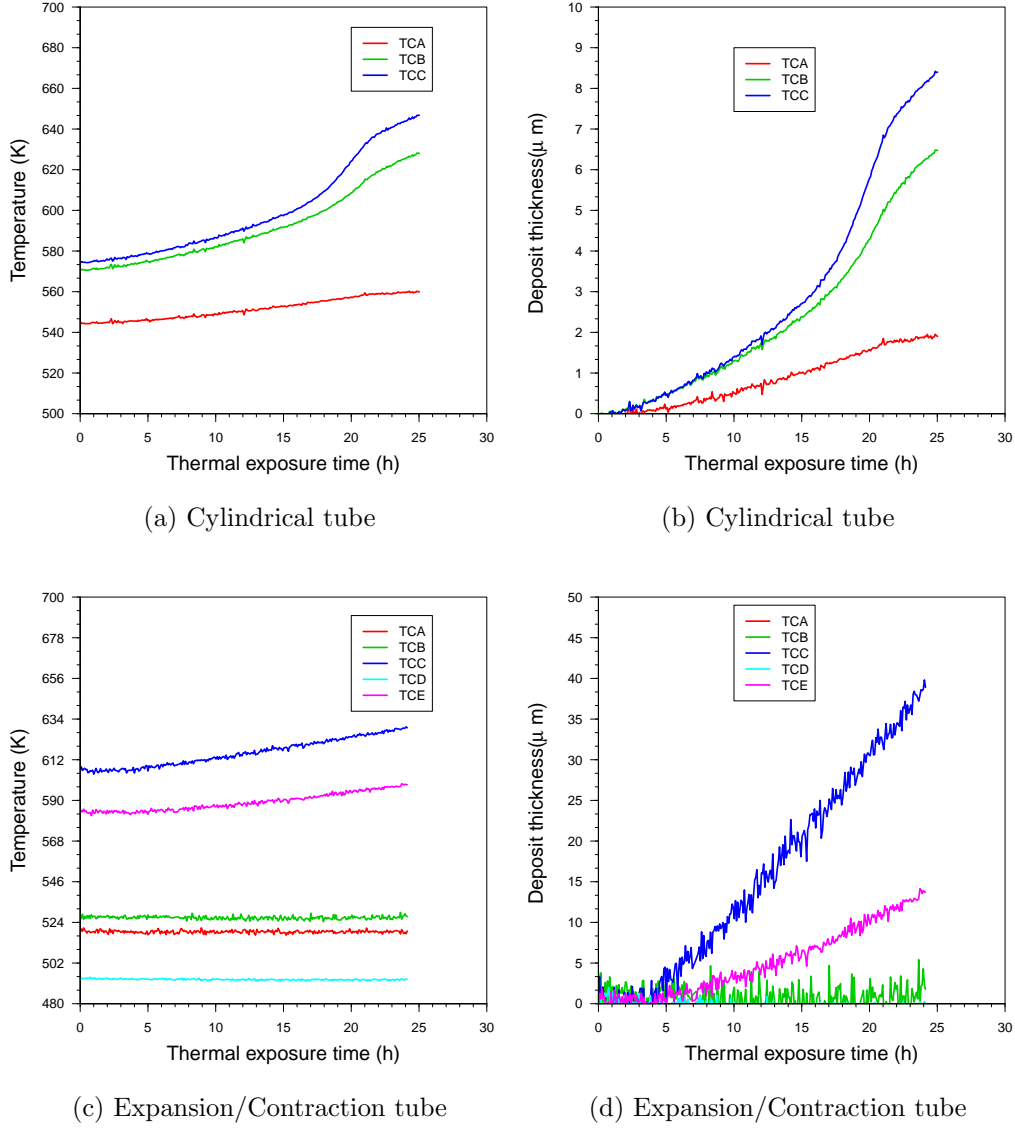


Figure 4: Temperature rise recorded by the thermocouples and corresponding calculated deposit thickness

Figures 5a and 5b present the simulated temperature profiles along the inner surface of the replicated straight feed arm and feed arm with expansion/contraction respectively. It is shown that for the feed arm with expansion/contraction structure, more accurate results was achieved with  $k - \omega(\text{SST})$  turbulence model to predict temperature at fuel wetted surfaces in the regions affected by tube enlargement while  $k - \epsilon$  lacked the accuracy [19]. The imprecision of  $k - \epsilon$  is evidenced by approximately 10 K tem-

perature difference at location corresponding to the first thermocouple(TA). This is of great concern as the accurate prediction of surface deposition is vastly sensitive to the simulated values of temperature along the inner surface where deposits build up. However, the differences obtained by the change of turbulence models for straight feed arm were trivial. The grid dependency was performed for both expansion/contraction and straight pipe simulations to ensure that calculations are independent of computational mesh numbers.

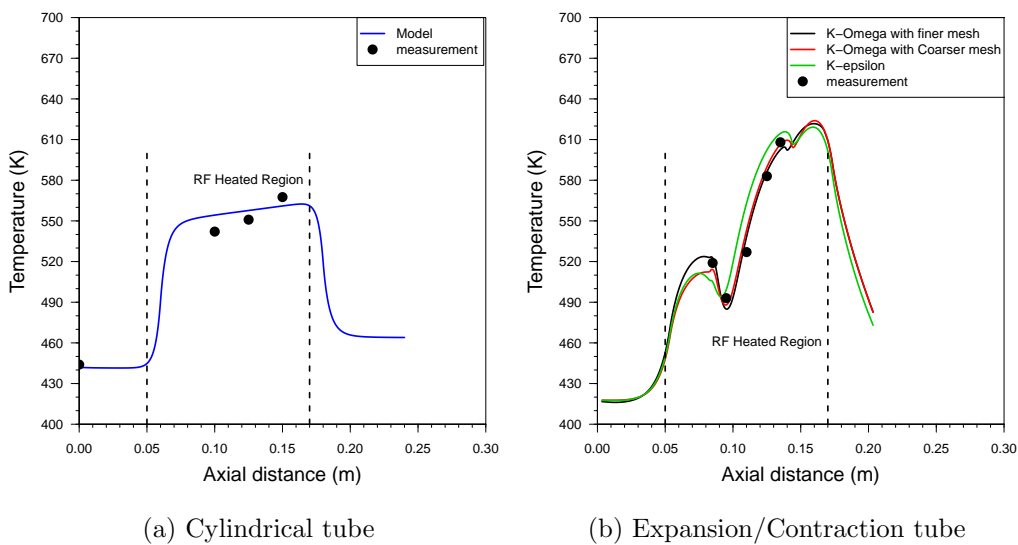


Figure 5: Validation of CFD models with experiments data obtained from Test1 and Test2

Figure 5b shows that approximately 75 k temperatures rise occurred along the tube inner surface of feed arm with expansion/contraction structure from an axial location of 50 mm to 80 mm. This is due to the effect of inductive heat generated by the RF unit. This is followed by almost 35 k temperature drop over the next 20 mm along the inner surface. Such temperature drop is attributed to the formation of strong recirculation zone created by the impact of tube diameter enlargement on flow regime as shown in figure 6. It is envisaged that at the expansion entrance, fluid emerging from smaller diameter is unable to follow the sudden deviation of the boundary. This results in creation of stagnant flow at the tube corner. [20] The stagnant flow remains in contact with the heated surface for longer which in turn results in a fluid temperature rise. The temperature rise in the recirculation zones is greater than value of cylindrical tube. The drop in the heat transfer coefficient in the recirculation region of the tube following the step causes increase in wall

temperature. As a consequence, hotter fluid region reduces temperature gradient between the wall and flow and hence, reduces the conductive heat flux from the wall in the region. This seems to insulate the wall with a hot fluid film, which increases the axial heat transfer through the metal body which results in temperature to peak prior to the expansion entrance as shown in figure 7b and figure 5b. The same phenomenon occurs at the tube corner where expansion ends. Downstream of the tube enlargement, the vigorous mixing caused by the turbulence helps to smooth the flow and practically after position of thermocouple B (15 mm after tube enlargement) the flow becomes uniform over the tube cross-section as shown in figures 8a- 8f. As shown in figure 9, immediately after sudden contraction, a vena contracta forms after which at some distance, flow stream widens again to fill the pipe.

In contrast to the complex flow regime and heat transfer characteristics caused by expansion and contraction, the replicated straight feed arm presents more simplistic situation. The results shown in figure 7a and figure 5a indicate that along the tube inner surface temperature begins to increase sharply from around 440 k at approximately 100 mm axial distance to about 540 k over 10 mm length. This temperature rise is due to the effect of inductive heat generated by RF unit which is followed by a moderate temperature rise to 564 k for the rest tube inside the RF heating unit, point corresponding to 220 mm axial distance. Beyond this point temperature decreases substantially to 473 k due to natural convection over 30 mm tube length. These results are collectively predictable as flow is fully developed for the entire computational domain and there is no change of flow direction to alter the heat transfer rate.

The collection of microscopic images of surface deposits corresponding to the axial location of thermocouples is shown in figure 10. It can be seen that despite the long residence time that stagnant flow is exposed to at tube corner after enlargement, the amount of deposit at this region is trivial. This indicates that the formation of deposit is extensively sensitive to the temperature at fuel wetted surfaces. It can be concluded from the results that surface deposition becomes more severe at thermocouples C and E where the wall inner temperature is the highest. The results pertinent to the thermocouples C and E are in support of one dimensional heat transfer calculation for deposit thickness.

The zonal carbon burn off analysis for both cylindrical and expansion contraction tubes are presented in figure 11a. Dimensions and location of each segment is shown in figure 11b. For cylindrical tube, it is shown that the

maximum amount of carbonaceous deposits is accumulated in zone2 where the highest temperature rise are evident in the wall corresponding to the thermocouple B and C locations. Similarly, for expansion/contraction tube, the maximum amount of carbonaceous deposit is accumulated in zone2 the section with highest measured temperature. Total amount of deposit for expansion/contraction tubes is markedly higher than the cylindrical tube.

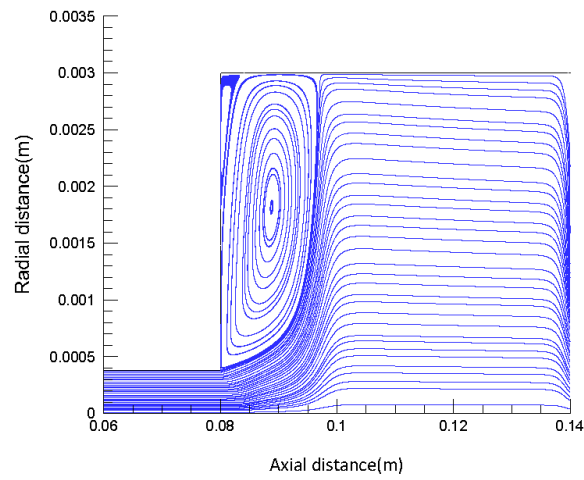
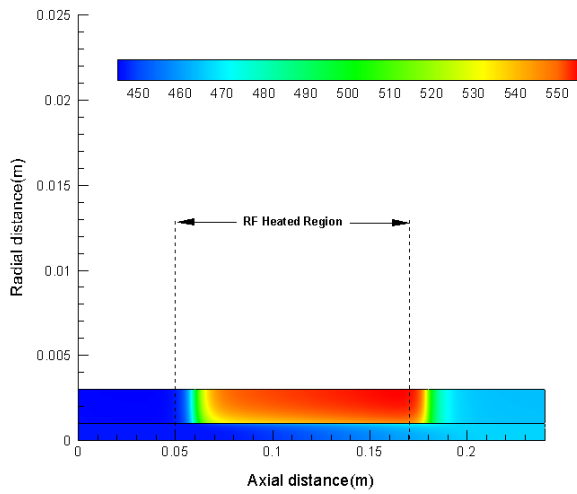
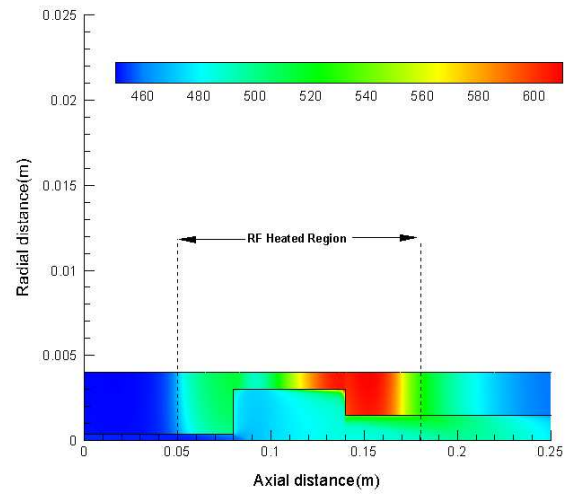


Figure 6: Contour of streamlines along the heated nozzle including expansion/contraction-geometry was zoomed in for clear graphical presentation

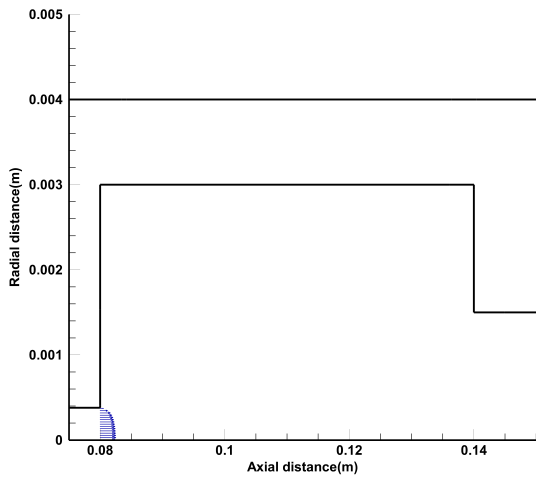


(a) Cylindrical tube

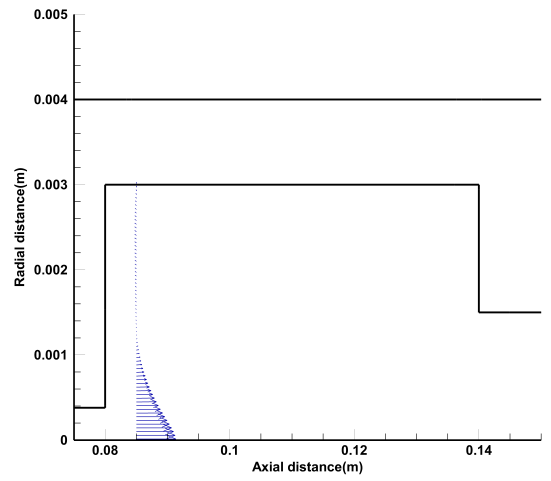


(b) Expansion/Contraction tube

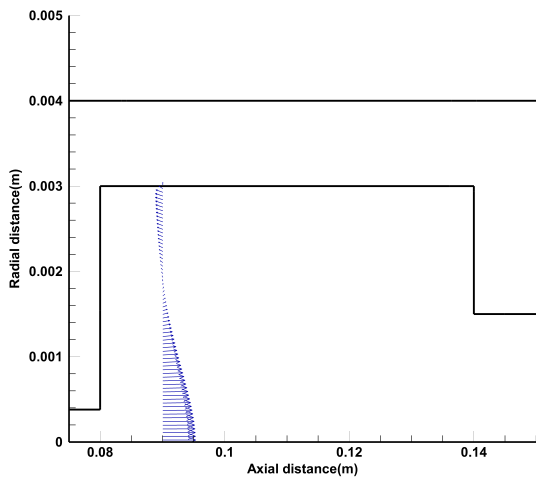
Figure 7: Contour of temperature profile in expansion/contraction and cylindrical tube, enlarged in radial direction for better graphical presentation(not to scale)



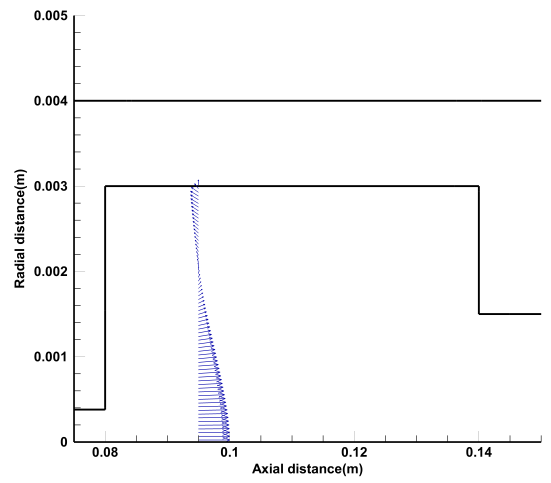
(a)



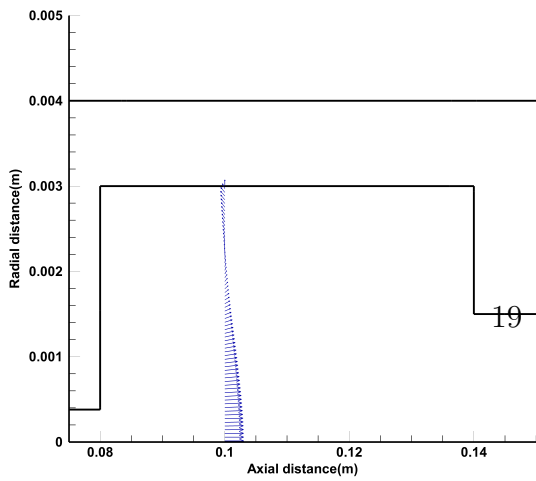
(b)



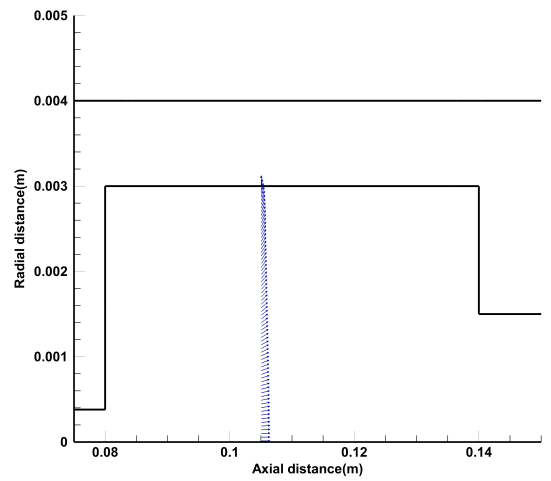
(c)



(d)



(e)



(f)

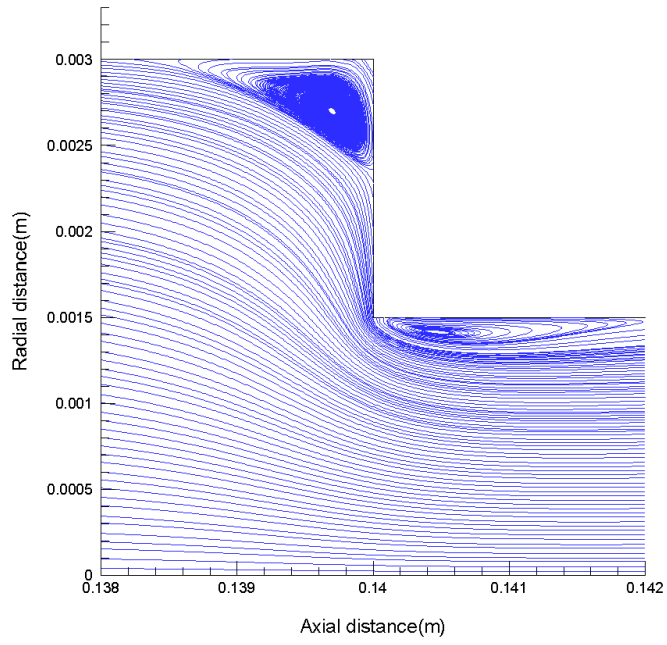


Figure 9: Contour of streamlines showing formation of vena contracta after tube contraction, zoomed in for better graphical presentation

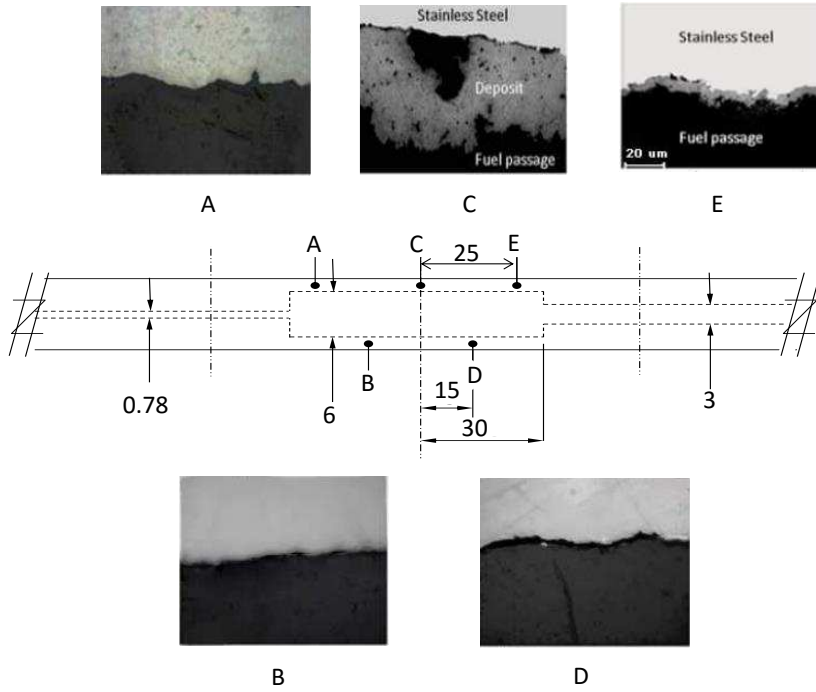
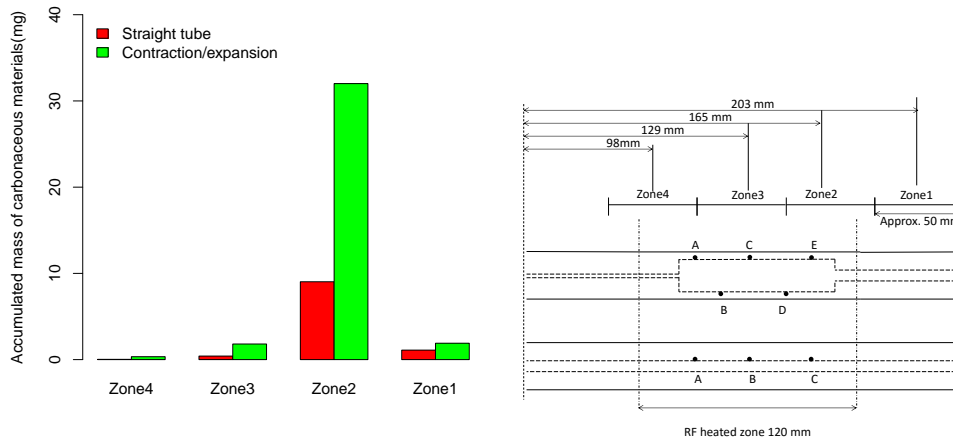


Figure 10: Collection of microscopic images of surface deposits corresponding to the axial location of thermocouples, schematic not to scale



(a) Quantified carbon deposit along the tubes (b) Locations of segments along the tubes-not to scale

## 5. Conclusion

The formation of surface carbonaceous deposits was investigated in a replicated feed arm burner with contraction/expansion structure in an aero engine representative condition provided by the AFTSTU. The replicated feed arm burner represents one of the geometrical features found in modern burner feed arms. The amount of deposit was measured in four zones along the heated feed arm by carbon burn off analysis. Furthermore, optical microscopy was used to directly measure deposit thickness at certain axial locations along the heated tube. The latter was used to validate a simple one dimensional mathematical model for estimation of deposit thickness based on the temperature rise along the tube wall. The experimental results were subsequently compared with surface deposits formed under the same test conditions in a replicated feed arm burner with cylindrical structure of the same length and inlet/outlet diameter. Computational fluid dynamic models were used to interpret the effect of tube enlargement and contraction on fluid flow and heat transfer characteristics and eventually on surface deposit formation. The more extensive discussion about heat transfer and fluid flow along with the chemistry of surface deposition will be presented in the volume II of this work.

## 6. Acknowledgment

This paper is based on research sponsored by 7<sup>th</sup> Framework Programme for Research and Technological Development, under grant agreement 211843.

- [1] Hazlett, R N, Thermal Oxidation Stability of Aviation Turbine Fuels, ASTM, 1991.
- [2] E. G. Jones, W. J. Balster, Phenomenological Study of the Formation of Insolubles in a Jet-A Fuel, *Energy & Fuels* 7 (10) (1993) 968–977.
- [3] W. F. Taylor, Development of High Stability Fuel, ESSO Research and Engineering Report, Tech. rep., Department of the Navy; Naval Air Systems Command (1972).
- [4] D. R. Kendall, G. Houlbrook, R. H. Clark, S. P. Bullock, C. Lewis, Injector Feed Arm Fouling- Part 1, Results from a Full-scale Rig, in: 30th International Gas Turbine Congress, Paper 87-IGTC-49, 1987.
- [5] S. Zabarnick, Chemical Kinetic Modeling of Jet Fuel Autoxidation and Antioxidant Chemistry, *Industrial & Engineering Chemistry Research* 32 (1993) 1012–1017.

- [6] S. Zabarnick, Pseudo-Detailed Chemical Kinetic Modeling of Antioxidant Chemistry for Jet Fuel Applications, *Energy & Fuels* 12 (97) (1998) 547–553.
- [7] N. J. Kuprowicz, J. S. Ervin, S. Zabarnick, Modeling the liquid-phase oxidation of hydrocarbons over a range of temperatures and dissolved oxygen concentrations with pseudo-detailed chemical kinetics, *Fuel* 83 (13) (2004) 1795–1801. doi:10.1016/j.fuel.2004.03.013.  
URL <http://linkinghub.elsevier.com/retrieve/pii/S0016236104001103>
- [8] N. J. Kuprowicz, S. Zabarnick, Z. J. West, J. S. Ervin, T. Edwards, Use of Measured Species Class Concentrations With Chemical Kinetic Modelling for the Prediction of Autoxidation and Deposition of Jet Fuels, *Energy & Fuels* 21 (2007) 530–544.
- [9] D. L. Dagget, A. Veninger, C. Lewis, B. S., R. Kamin, The Development of an Aviation Fuel Thermal Stability Test Unit, *Journal of Engineering for Gas Turbines and Power* 117 (1995) 468–473.
- [10] S. Siouris, S. Blakey, C. W. Wilson, Investigation of deposition in aviation gas turbine fuel nozzles by coupling of experimental data and heat transfer calculations, *Fuel* 106 (2013) 79–87. doi:10.1016/j.fuel.2012.12.006.  
URL <http://dx.doi.org/10.1016/j.fuel.2012.12.006>
- [11] H. Jiang, J. Ervin, S. Zabarnick, Z. West, Effects of Flow Passage Expansion or Contraction on Jet-Fuel Surface Deposition, *AIAA Journal of Propulsion and Power* 28 (4) (2012) 694–706. doi:10.2514/1.B34356.  
URL <http://dx.doi.org/10.2514/1.B34356>
- [12] D. Boss, R. N. Hazlett, R. L. Shepard, Analysis of n-Paraffin Oxidation Products in the Presence of Hydroperoxides, *Analytical chemistry* 45 (14) (1973) 14–18.
- [13] Z. J. West, S. Zabarnick, R. C. Striebich, Determination of Hydroperoxides in Jet Fuel via Reaction with Triphenylphosphine, *Industrial & Engineering Chemistry Research* 44 (10) (2005) 3377–3383. doi:10.1021/ie0490379.  
URL <http://pubs.acs.org/doi/abs/10.1021/ie0490379>
- [14] H. W. Fink, Donald G.; Beaty, *Standard Handbook for Electrical Engineers*, McGraw-Hill, 2000.

- [15] M. R. TeVelde, J A., Glickstien, Heat Transfer and Thermal Stability of Alternative Aircraft Fuels, Tech. rep. (1983).
- [16] E. Alborzi, G. S. Blakey, H. Ghadbeigi, C. Pinna, M. Pourkashanian, C. Wilson, Analysis of the Structure of Deposited Materials at Inner Surface of Jet Fuel Injector Feed Arm With Optical and Scanning Electron Microscopy, in: IASH 2011, the 12th International Conference on Stability, Handling and Use of Liquid Fuels, Sarasota, Florida USA. October 16-20, 2011.
- [17] V. R. Katta, R. W. M., Numerical Method for Simulating Fluid-Dynamic and Heat Transfer Changes in Jet Engine Injector Feed Arm Due to Fouling, *Journal of Thermophysics and Heat Transfer* 7 (1993) 651–661.
- [18] Incropera, F P. and David, P Dewitt. and Theodore, L Bergman. and Adrienne, S Lavine , *Introduction to Heat Transfer*, 5th Edition, Wiley, 2005.
- [19] TU, Jiyuan. and Yeoh, Guan Heng. and Liu, Chaoqun, *Computational Fluid Dynamics: A Practical Approach*, 1st Edition, Elsevier Inc., 2008.
- [20] Massey, Bernard, *Mechanics of Fluids*, 7th Edition, Nelson Thornes Ltd, 2001.